Pump as turbine applied to micro energy storage and smart water grids: A case study

Alessandro Morabito*, Patrick Hendrick

Aero-Thermo-Mechanics Dept. (ATM), École Polytechnique, Université Libre de Bruxelles (ULB), Belgium

HIGHLIGHTS

- A novel micro-PHES prototype system installed in a smart grid is presented.
- Energy storage and energy recovery achieved via a single centrifugal pump.
- The set-up and the pump selection solution form are presented.
- A round-trip energy efficiency of 42% is achieved with variable speed regulation.
- Levelised cost of energy of the micro-PHES case study is 1.06 €/kWh.

ARTICLE INFO

ABSTRACT

The need of energy storage in micro scale is recently emerging and becoming more relevant in the rising era of decentralised renewable energy production. This paper provides a technical overview of the design and the outcomes of a first-of-its-kind Pumped Hydro Energy Storage (PHES) micro facility. The described micro-PHES is integrated in a smart grid and it is designed to store energy produced by the connected renewable energy sources. Interestingly, this micro-PHES runs with a single centrifugal pump for both pumping and generating phases. Variable speed regulation allows the pump to constantly operate at the maximum hydraulic efficiency in order to deal with load variations. In the same way, the pump running in reverse, namely Pump as Turbine (PaT), runs at the most suitable speed and it keeps high efficiency (near to 0.71%) over a range of 40–120% of the nominal load design. The pump/PaT is selected according to the presented methodology and it is experimentally characterized in the current case study. The PHES implementation is defined in relation with the smart grid consumption and renewable energy production and it reaches a total round-trip yield up to 42%. In addition, this paper defines the techno-economic parameters for a micro-PHES cost-effective solution and provides an important dataset for micro-PHES feasibility breakdown. The use of a storm-water basin as reservoir produces an expense cut greater than 28% of the total direct cost. This constitutes a valid economic advantage to be integrated in future smart water grid's designs. Also, the system with the described features can reach a Levelised Cost of Energy (LCOE) of 0.58–1.06 €/kWh in micro-PHES.

1. Introduction

At the end of 2017, global renewable generation capacity amounted to 2179 GW [1]. This continued the recent trend of an 8–9% yearly increase in renewable energy, including a capacity increase of 94 GW (+32%) for photovoltaic (PV) panels and an increase of 47 GW (+10%) for wind energy [1]. In Europe, the renewable energy share growth was 24 GW (+4.8 This represents considerable progress in reducing fossil fuel usage and meeting long-term reduced greenhouse gas emissions targets [2].

Nevertheless, a significant drawback to solar and wind energy is its intermittent production due to seasonal or even daily changes in the weather. As a consequence, there is often a mismatch between renewable energy production and its use. In remote areas, this usually leads to the installation of fossil-fuel energy sources such as diesel engines to supply the base-load demand. The integration into the electricity network of a small number of decentralised (and occasionally large) renewable power plants (photovoltaic, wind) is therefore a major challenge for the network's stability and flexibility [3]. Answers to these problems need to include the interconnection of European transmission

* Corresponding author at: Université libre de Bruxelles, Av. F. D Roosevelt 50, Brussels, Belgium.
  E-mail address: alessandro.morabito@ulb.ac.be (A. Morabito).

Nomenclature

C	cost (€)	μ	dynamic viscosity (Pa s)
d	yearly discount rate	π	power number
D	diameter (m)	ρ	density (kg/m^3)
E	energy (kWh)	φ	discharge number
F	scalable loss fraction	ψ	correction coefficent
H	head (m)	ω	angular speed (rad/s)
K	project duration (years)	Ψ	head number
l	length (m)		
L	pipeline length (m)	*Subscripts*	
N	rotational speed (rpm)		
N_s	specific speed (m, m^3/s)	l	loss
Q	flow rate (m^3/s)	*max*	maximum
M	angular momentum (Nm)	*min*	minimum
T	temperature (°C)	*opt*	optimum
v	fluid speed (m/s)	*out*	output
V	volume (m^3)	p	pump mode
η	efficiency	*rw*	runaway
λ	efficiency ratio	t	turbine mode
		th	theoretic

networks, the dynamic management of power demand and storage, and a strengthening of the power lines [4]. Pumped Hydro Energy Storage (PHES) is a very important solution to the problem of energy storage. Worldwide PHES capacity is about 55 GW in Europe and over 170 GW worldwide, representing the 97% of the total energy storage capacity [5]. Traditionally this system consists of two dedicated reservoirs at different height levels linked by a pipeline, a pumping system and hydraulic turbines. During off-peak demand, PHES pumps water up from the lower reservoir. The potential energy stored in the upper reservoir is then used by a hydraulic turbine group when needed. The PHES systems are robust and use mature technologies. Although needing a large area, they can easily be installed and maintained. They do not emit greenhouse gases and can be largely disassembled at the end of their working life. Today, PHES is certainly one of the most ecological options for electric energy storage notwithstanding a few negative impacts on the land [6,7].

The performance of a PHES site is clearly dependent on the turbomachinery used and is sensitive to each specific local scenario [8]: pumps and turbines have to be installed according to the exploitable flow rate, available head and pipeline system characteristic curve. Although pumps and turbines are designed for a particular flow rate, they operate across a certain range due to the fluctuation of the available head and/or load (like filling a tall column of water from the bottom). The water level may vary through the full cycle of reservoir emptying and filling according to its specific geometry and the flow regime.

The problems associated to micro scale units (μ-PHES) are different than in large PHES units. The issues related to operation, maintenance and repair technologies are critical for the micro scale (5–100 kW of power production). Manolakos et al. [9] illustrate a μ-PHES on Donoussa Island, Greece, coupled with an 18 kW-peak (kWp) photovoltaic power system. The micro-hydraulic system consists of a pump and a hydraulic turbine of 7.5 kW and two identical water reservoirs of 150 m^3 capacity each with a height differential of about 100 meters. Another hybrid system with PV and a co-generative internal combustion engine is coupled with lead-acid batteries and thermal and water storage, to satisfy the energy and water needs of a small isolated touristic resort in Northern Italy [10]. PHES technical feasibility and its economic comparison with other promising storage technologies are discussed on a small scale by Silva and Hendrick [11]. It appears that high cost and low efficiency compromises the competitiveness of PHES on small scales [11]. Battery price and reliability is however improving rapidly, mainly driven by the automotive industry: plug-in hybrid and electric car sales exceeded 3 million in 2017, up 54% from 2016 [12].

Relevant design decisions can be taken to reduce the costs and improve the performance based on traditional PHES concepts. This paper describes the unique nature of installed μ-PHES and the methodology used in the selection of the PaT according to the specifications of the storage system. The μ-PHES designed and here analysed has a closeloop configuration, which consist of two reservoirs that are isolated from a free-flowing water source. Thus, the generated energy comes solely from the storage of renewable sources. The chosen pump must be able to pump water to the upper reservoir and to work in reverse mode (Pump as Turbine or PaT) at high efficiency by means of rotational speed adjustments.

PaTs are most applicable to micro hydropower stations from natural water streams in rural areas [13], but also to urban water distribution networks, exploiting the excess of energy that can be present along any branch of the system [14]. The pressure along the distribution network has to be kept in balance. Usually valves are used to dissipate this excess of energy, but PaTs are an interesting technical solution which ensures both economic convenience and system flexibility [15]. The introduction of PaTs in the water-energy network has large potential in promoting energy savings practises [16]. One of the key advantages of PaT is that it can have a payback period 5 times shorter than for conventional micro hydro-turbines, although PaT hydraulic efficiency is usually reported as being lower [17]. Economically, PaTs below 500 kW are profitable in hydropower and allow capital payback periods of about two years [18,19]. PaTs thus provide a solution for those hydropower sites in which conventional turbines might not be affordable. For decades researchers discussed the hydraulic behaviour of pumps in reverse mode and tried to formulate a function or a model able to define the hydraulic performance. A collection of proposed correlations is summarized in dedicated reviews [20,21].

The objective of this paper is to explore the performances of a unique μ-PHES system equipped with a single pump in a smart grid scenario. This paper presents data of real-life pumped energy storage application in micro scale, using technical and material synergies that have not been discussed together before:

- instead of having a group of pumps for charging and a separate group of turbines for generating, the adopted solution (a single pump for both modes) reduces the number of hydraulic machines needed and reduces the space required for pipeline fittings, thereby cutting costs. The literature describes experimental studies of PaT model prediction formulations but errors in the sampled efficiency evaluation used for the correlation are at 25–30% [22–24]. Further

research and data to accurately calculate the PaT performance model are thus needed and here provided. The turbomachine selection method is applied and discussed and integrated with the methodology implementation of pump/PaT operation in μ-PHES.

- Load fluctuation and operational flexibility have become a new orientation [25] within the targets of rentability and high efficiency [26,27]. Hence, evaluating the advantages and demonstrating the additional value of speed regulation is a relevant and practical topic [28]. In the present study, a variable frequency driver is coupled to the motor/generator in order to change from pumping to generating mode and to react efficiently to the load fluctuation. This has been managed via monitoring the energy consumption profile of the smart grid.

- Pumped storage plants are characterized by high capital expenditure and the excavation costs, where needed, constitute one of the greater direct expense [29,30]. Methods of exploiting water distribution network [14] and underground cavities [31] for hydroelectricity production have been previously modelled in the literature. Few other methods have been simulated in micro storage application as in aquifers and flooded quarries [32] or residential areas [33,34]. In the presented μ-PHES a storm-water basin is concretely implemented as a cost-effective solution for a water reservoir.

The existing literature on PHES describe the technology in details [3,35], but information about real-life application are still needed [36,37] especially in micro-size [11]. Moreover, this paper defines the techno-economic parameters for a micro-PHES cost-effective solution. A Levelised Cost of Energy (LCOE) analysis provides an important dataset for micro-PHES feasibility breakdown.

This paper is structured as follows: Section 2 starts with an overview of the smart grid where the PHES is installed. The PaT selection methodology is then discussed and the set-up application is described. Section 3 presents the results of the experimental investigation of the hydraulic system performance and on the use of variable speed. A cost-benefit analysis is described in Section 4, followed by the conclusions.

2. Material and methods

2.1. Micro-PHES in "le quartier Negundo"

The PHES case study is located in Froyennes, Belgium (Fig. 1). It is integrated into a smart grid agglomerate, which includes offices and conference centres, called Negundo ("*le quartier Negundo*"). Several buildings in this district have an interconnected power supply network as well as sharing various sources of wind and solar energy. The μ-PHES is managed by IDETA (Agence de Développement Territorial - Territorial Development Agency) with the collaboration of the Aero-Thermo-Mechanics Department at the Université libre de Bruxelles. IDETA gives technical and administrative support to businesses to help them set-up and/or develop their project plans. IDETA has also shown an increasing interest in renewable energy sources and energy efficiency by partnering several projects concerning solar, wind, biomass, hydro energy sources and electric vehicles.

The micro energy grid, illustrated schematically in Fig. 2, has different renewable energy sources which support the energy consumption in the connected buildings. In Negundo, a solar flower of 5.2 kWp and two other groups of photovoltaic panels of 10 kWp and 15 kWp are installed. Four wind turbines of 2.4 kWp each are also present. 60 kWp building integrated PV panels are installed and an adjacent solar carport facility provides 20 kWp. The μ-PHES (of about 17 kWh) is equipped with a single PaT that provides a peak of 7 kW production. The maximum theoretical amount of energy stored, namely capacity E in kWh is given by

$$E = \rho V g H / 3600 \qquad (1)$$

where ρ is the water density and g is the gravity acceleration. In a more accurate way, the energy produced is product of the capacity and the total efficiency of the system in generation mode, $E_t = E\eta_t$. The amount of energy consumed in storing energy in the whole upper reservoir is equal to the capacity over total efficiency of the system in pumping mode, $E_p = E/\eta_p$. To design PHES, the capacity of the site has to be defined according to the available water volume V in m^3 and head H in m. About 650 m^3 are available from a storm-water basin used to collect run-off water from local roofs and roads in order to prevent flooding or erosion. Storm-water basins (or retention basin) - as frequently used in rural and in urban areas for flood prevention and management - provide a vegetative buffer that can withstand dry or wet conditions. They constitute an innovative solution to be applied in hydroelectricity and energy storage systems. Due to its location, this basin is used as the upper reservoir for the μ-PHES (Fig. 3). The lower reservoir, conceived as an extension of the storm-water basin, has been built with a capacity of 650 m^3 next to one of the buildings in the street block (Fig. 4). Building the reservoir out of prefabricated water-resistant concrete components simplifies both its installation and maintenance, which would not be possible if it was made from a series of single interconnected tanks.

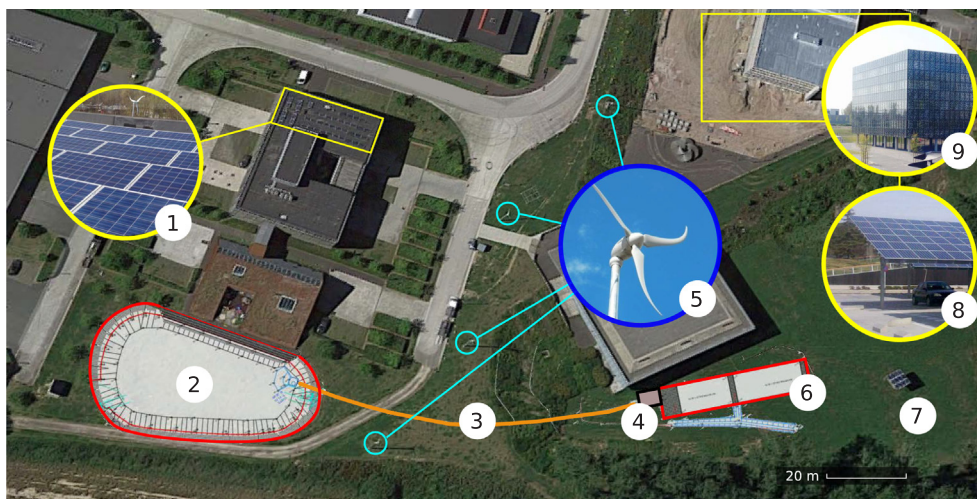Unlike the upper reservoir, which is wide and not very deep (about

Fig. 1. View of the *quartier Negundo*: 1. PV panels; 2. Upper storm-water reservoir; 3. Pipeline; 4. Technical room; 5. Micro wind turbine; 6. Lower storm-water reservoir; 7. Solar flower; 8. Solar carport; 9. Building integrated PV panels.
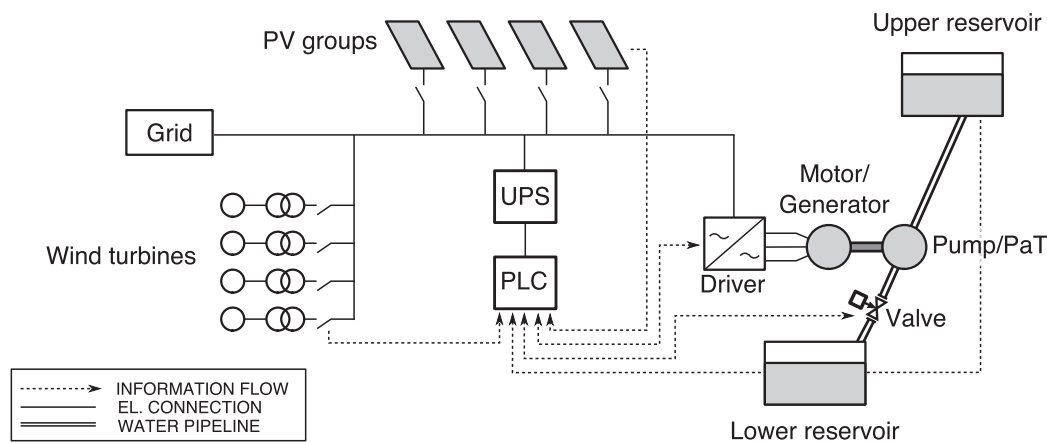
Fig. 2. Interconnection scheme of *quartier Negundo* smart grid.

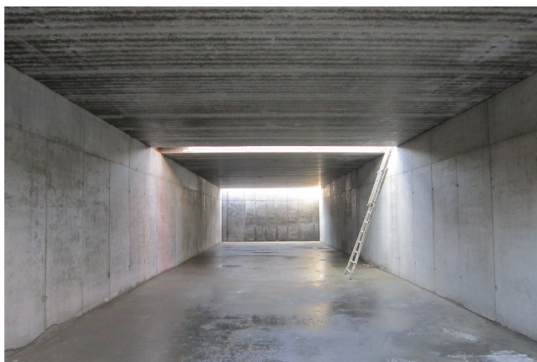**Fig. 3.** View of the upper reservoir in *quartier Negundo*.

Fig. 4. Internal view of the lower reservoir of the μ-PHES.

1 meter), the lower reservoir needs to fit among the existing building in the surrounding area. Due to its geometry (deep and narrow), its water level varies considerably during the normal working cycle of charging and discharging. In fact, the water level fluctuation (about 3 meters) is relevant to the modest maximum differential height (11 meters). In order to deal with a possible severe variation of the available head, a new feature has been tailored to this μ-PHES. A Variable Frequency Driver (VFD) is coupled to the turbomachine, allowing the pump to rotate in inverse direction when working as a turbine. If it were not for the working condition variations, a gear-box would provide two rotational speeds on the shaft: one suitable for pumping and the second applied for generating mode, but any speed adjustment would be possible. The VFD modulates the rotational speed in order to operate at high efficiency under the changing working conditions: the most suitable rotational speed can be selected for the available head. As well as dealing with load fluctuation, there are other major advantages of

variable speed generation. The high inrush current at the start is remarkably reduced and gradual changes are produced in the flow that do not upset the normal functions of the system. In addition, having fewer start-ups avoids power dips, reducing the need for system maintenance as a result of the wearing of bearings and flexing of the shaft. Variable speed control does however add extra cost and complexity to the system.

The Programmable Logic Controller PLC system is equipped with an uninterruptible power source (UPS) to guarantee a safe shut-down procedure in case of main power fail. In unexpected power disruption or error event, the commands of shut down the electric machine and closing the valve are sent as an alarm message.

2.2. Pipeline and pressure losses

The two reservoirs are connected by about 80 meters of pipeline, with an internal diameter of 355 mm made from PE100, which provides long-term strength, creep resistance and a low friction coefficient. In the technical room, where the pump is installed, the pipes are made of stainless steel and the diameter reduced to 200 mm (pump discharge side) and 250 mm (at pump suction side). The pipeline sinks more than 8 meters and has to cross under a bank, a pedestrian way and a sewer line. For these reasons, it has not been possible to keep the penstock outside or to bury it as usually done. Instead, directional drilling practice has been employed, adding additional cost to the pipeline installation. From the upper reservoir, a well is piloted to reach the technical room that would otherwise be inaccessible with traditional drilling practices. According to the Colebrook-Prandtl relation [38], the head loss due to the losses in the straight pipe (in polyethylene) is about 0.6 m at the maximum measured flow rate (133 kg/s). Local pressure losses are also produced by the different fittings of the pipeline. Two grids protect the pump from external objects at the price of further losses (about 0.2 m each) and a flanged diffuser is necessary to connect two pipes of different diameters. In order to reduce these undesirable effects two diffusers are installed on each pipeline inlet.

2.3. Turbomachinery selection

In hydropower plants conventional hydro-turbines are selected based on their available head, *H*, and flow rate, *Q*. Pelton and Turgo impulse turbines of varying sizes are perfectly suited to high-head hydroplants and reaction turbines such as Francis, mixed-flow, Kaplan and bulb turbines can function over a wide range of available head and flow rate. Recently in micro-hydropower plants (⩽100 kW), PaT can be found with downsized impulse turbines, reaction turbines and Cross-flow turbines (Fig. 6). Compared to large turbomachines, the behaviour of small pumps in reverse mode is quite different: as an industrial

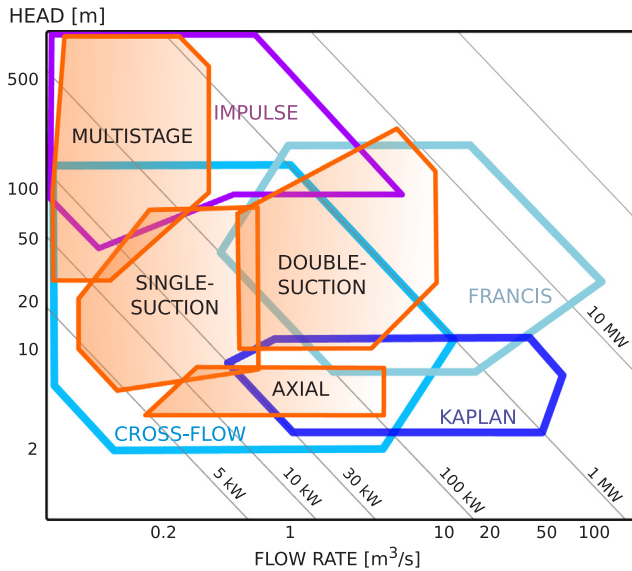**Fig. 5.** Centrifugal PaT installed in the technical room next to the lower reservoir.

Fig. 6. Types of hydraulic turbines and PaT (multistage, single suction, double suction and axial type) in their application area Q-H for micro-hydropower. Adapted from [39,40,18,41].

pump, PaT design does not have any particular need to run in reverse mode unlike pump-turbines used in large PHES [42]. Moreover, PaTs are not usually equipped with fixed/movable guide-vanes which are used in turbines for directing the flow: in PaTs only the volute operates as the water flow guide [43]. Different series of PaTs can be selected according to the performance required and the efficiency curve itself is affected whether a PaT is operating off-grid [16]. With regard to the flow and pressure, multi-stage PaTs for high head and double suction PaTs for high flow rate can be selected (Fig. 6).

In the case study the exploitable available head is not very large and varies considerably during a whole cycle. A traditional hydro-turbine would have been too expensive [17] and it would often operate in off-design conditions, reducing the overall system efficiency. To overcome these difficulties, a single pump is selected in order to charge the upper reservoir but it is able to run in reverse, as a turbine, to generate hydroelectricity. The pump must obviously be able to recharge the upper reservoir up to at least $H_{p,max} = H_{th} + H_{max,l}$. The manufacturer catalogues provide the Q_p, H_p and N_p.

The prediction models focus on the definition of the head and flow of the Best Efficiency Point (BEP) in reverse mode. The ratios $h = H_t/H_p$ and $q = Q_t/Q_p$ relate the BEP working condition in pump mode with the turbine mode at the same rotational speed. It appears that PaTs usually have a BEP located at higher flow rate and higher head compared to the normal pumping operation at the same rotational speed [13]. Thus, the

fluid power (proportional to the product of H and Q) engaged by the turbine would be higher than the power employed by the pump rotating at the same speed, assuming an identical efficiency. The pump hydraulic efficiency is fundamental for the formulation of several prediction models: Alatorre-Frenk [44], Childs [45], Schmied [46], Sharma [47], Stepanoff [48]. Other predictive models are based on the specific speed, N_s [49–51], which describes the runner or impeller of a turbomachine linking mass flow rate, rotational speed and energy. Recently, one-dimensional numerical codes have become available to estimate the performances of centrifugal PaTs [52] although they require highly detailed information which is not easy to get.

A statistical/empirical method is used here. Subgroups of tested pumps, defined by the impeller diameter, lead to a better match with the experimental values of h and q in the literature [51,43]. According to the manufacturer catalogue, pumps between 0.25 m and 0.30 m impeller diameter suit the requirements in Q and H on the Froyennes site. For this pump impeller range, the following equations, depending on the pump specific speed, $N_{s,p}$, are found [53]:

$$h = 5.196 N_{s,p}^{-0.323} \qquad q = 3.127 N_{s,p}^{-0.219} \qquad (2)$$

The pump specific speed

$$N_{s,p} = \frac{N_p \sqrt{Q_p}}{(H_p)^{0.75}} \qquad (3)$$

is calculated based on the pump BEP and thus, the ratio h and q are obtained.

As stated before, q and h are usually greater than one, which locates the PaT BEP at a higher flow rate and required head. A new rotational speed value must be set in order to match with the actual head offered on site $H_t = H_{th} - H_l$. For this passage, the so-called affinity laws help us to determine the new flow, head and power. The affinity laws, which are actually corollaries of Buckingham Pi theorem [54], define the non-dimensional groups

$$\varphi = \frac{Q}{UR^2} \qquad \psi = \frac{gH}{U^2} \qquad \pi = \frac{P}{\rho U^3 R^2} \qquad (4)$$

As long as these dimensionless parameters are maintained from application to application, it is possible to obtain a good prediction of the speed scaling by a resulting scale factor. The direct scaling yields with $D_a = D_b$ and $\rho_a = \rho_b$ are the following

$$Q_b = Q_a \frac{N_b}{N_a} \qquad H_b = H_a \left(\frac{N_b}{N_a}\right)^2 \qquad P_b = P_a \left(\frac{N_b}{N_a}\right)^3 \qquad (5)$$

Dimensionless parameters (Eq. (4)) are often used for turbomachinery scaling but the Reynolds number is also fundamental. The Reynolds number, Re, is the ratio of inertial forces to viscous forces of a fluid subjected to movement. Changes in the Re results in relevant hydrodynamic effects and losses. With this in mind, an efficiency correction for the modification due to PaT speed variation is necessary.

The transposition is in agreement with the methodology provided by International standard IEC code NO.60193 [55]. In this case, a reference Reynolds number of $7 \cdot 10^6$ is considered to minimize the deviation

$$(\Delta \eta_h)_{a \to b} = \delta_{ref} \left[\left(\frac{Re_{ref}}{Re_a}\right)^{0.16} - \left(\frac{Re_{ref}}{Re_b}\right)^{0.16} \right]$$

$$\text{with:} Re = \frac{\rho v l}{\mu} \qquad (6)$$

where $\delta_{ref} = (1 - \eta_{h,a,opt}) / \left[\left(\frac{Re_{ref}}{Re_{a,opt}}\right)^{0.16} + \frac{1 - F_{ref}}{F_{ref}} \right]$ with F_{ref} equal to 0.7 for operation as turbine and 0.6 for operation as pump [55]. The values of $\Delta \eta_{h,a \to b}$ divergences with the experimental results of 0.18%, within the data accuracy.

Another selection criteria in the PaT selection is the determination of the operating condition at torque $M = 0$ and, consequently at zero power output. This condition of no load defines the runaway

characteristic which connects all the points H(Q) which occur for $M = 0$ at various speeds. Gulich [56], defines the following equation for the runaway flow rate, Q_{rw}, and the runaway head, H_{rw}, by elaborating the data offered in [57–59]

$$H_{rw} = H_{t\,BEP}(0.55 - 0.002 N_{s,p}) \tag{7}$$

$$Q_{rw} = Q_{t\,BEP}(0.45 + 0.0067 N_{s,p}) \tag{8}$$

According to the affinity laws (Eq. (4)) with $Q_{rw} \propto N$ and $H_{rw} \propto N^2 \propto Q^2$, the runaway characteristic curve is obtained as a parabola through the origin of the coordinate system $H - Q$.

The numerical procedure for performance prediction and selection is illustrated in Fig. 7. Based on the characteristics of an available pump from the manufacturer's catalogue, the most suited performance prediction model can be used. The parameters h, q are defined as the parameter λ, which estimates the efficiency ratio η_p/η_t [51] (step 1). Thus, the working conditions of the selected pump in reversed mode rotating at the pump rotational speed are found (step 2). Applying the affinity laws, the rotational speed scaling is performed to suit to the site constrains: the flow rate and the available head are site depending (step 3). The revised rotational speed and best efficiency point are determined (step 4) and, by using the Eq. (6), the PaT hydraulic efficiency is adjusted (steps 5–6). In this iterative procedure, continuous checks must be performed to avoid cavitation phenomena and crossing runaway conditions. Minimum operating pump shaft speed is defined as that at which the pumping system is no longer able to deliver a positive flow rate against a static head. Hence, it is specific to each working condition. The minimum operating speed in reverse mode depends strongly on the running condition. According to the velocity flow angles at the inlet and outlet of the runner at the selected rotational speed, PaTs are able to deliver a power-output (torque $M > 0$) only above a minimum flow-rate, $Q_{PaT-min}$. Below this value, the PaT power output is negative. In other words, for $Q_{PaT-min}$ and consequently $H < H_{PaT-min}$, the power station is actually using energy to maintain the runner at the selected N. If possible, N should be re-set, when appropriate, updating the minimum values of $Q_{PaT-min}$ and $H_{PaT-min}$. The new operating condition at the set rotational speed must take into account PaT stability and the avoidance of incipient cavitation, if it does not, a new pump must be selected (step 7).

Concerning the case study, in the end, a centrifugal pump with an impeller diameter of 296 mm from Ensival-Moret/Sulzer was chosen (Fig. 5). The pump suction and discharge sides have diameters of 250 mm and 200 mm respectively. The specific speed of the selected pump at 1000 rpm results in 55 (rpm, m^3/s, m). This pump is in agreement with the specifics of the PaTs adopted for the formulation of Eq. (2). According to Eq. (2), the pump running in reversed mode at 1000 rpm has its BEP at 13.5 meters of head for about 117 kg/s of water. Due to the geographic limitation of the site, the system is not able to provide the required head to run the PaT at its estimated BEP. By the similitude given by Eq. (5), the rotational speed suitable for 6.5 meters available head is about 700 rpm and it will be provided by the VFD.

2.4. Set-up instrumentation

The system is monitored in order to measure the performance of the turbomachine in pump and in reverse mode. One pressure transmitter (Unik5000) is installed on the PaT inlet side and another one at the PaT discharge side. These pressure taps are manifolded (Fig. 8) and each tap is valved separately [60].

An ultrasonic flow-meter is installed upstream of the PaT where a sufficient straight pipe length is available to ensure a fully developed symmetrical flow profile. The ultrasonic flow-meter can be clipped directly onto the pipe and measures the flow rate in both directions. Mechanical torque and rotational speed measurements are obtained by a torque-meter mounted onto the turbine shaft. Water temperature is

measured in order to adjust the flow-meter setting as dependent on the sonic path and to alert to the possibility of ice formation in the volute, sealing and pipeline. When water freezes and becomes ice its expansion can be devastating. Ice growth at $-8\,^\circ$C can exert pressures as high as 92 MPa [61], pressures that not all the components of the pipeline and of the pump can withstand.

The signals outputs are connected to an acquisition card and managed by Labview for real-time measurement acquisition and control. The system is able to detect irregular flow by alarms from the driver, the presence of tension as well as from the flow-meter. The instrumentation range, accuracy and expected measurement ranges for the air side of the installation are listed in Table 1.

Since the PHES control system pilots the VFD via MODBUS and an electro-mechanic valve, it is possible to modulate the discharge rate and speed to best suit the operating conditions. Gradual changes are produced in the flow that do not upset the normal functioning of the system: the pump/PaT can be ramped up (or down) to reduce water hammer, which could have dangerous consequences on the integrity of the whole pipeline. If it were not for the variation of the working conditions, a gear-box would provide two fixed rotational speed on the shaft: one suitable for pumping and the second applied for generating mode.

2.5. Experimental methodology

The power generated and consumed by the pump installed in normal and reversed operation are

$$P_p = \frac{\rho g\, H_p Q_p}{\eta_p}, \qquad P_t = \rho g\, H_t Q_t \eta_t \tag{9}$$

where H_p and H_t are obtained by the total pressure gap measured in the pump discharge and in pump suction side. The flow rate is directly measured by the flow-meter, which is able to detect possible flow irregularities resulting from, for example, the presence of a mixture of vapour or air and water in the pipeline. Fig. 9 illustrates the schematic layout of the set-up and the positions of the pressure sensors (pressure
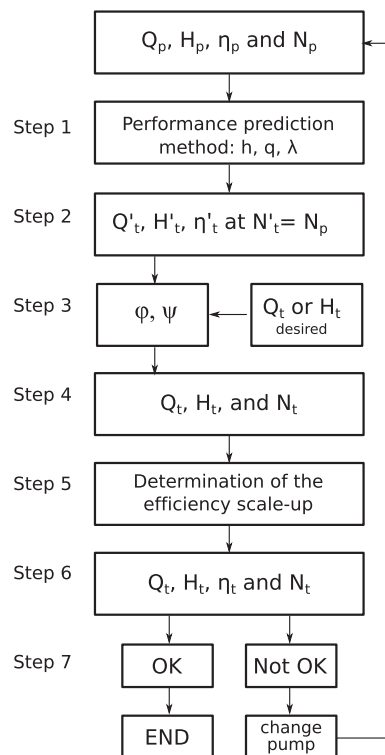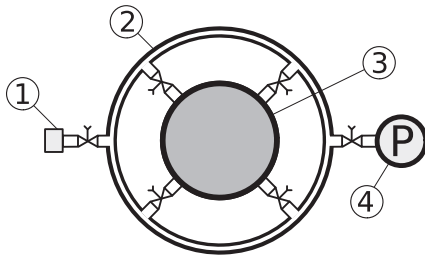

Fig. 7. Decision tree for PaT selection.

Fig. 8. Pressure transmitted manifold practise: 1. Air purge/drain; 2. Manifold ring; 3. Pipe section; 4. Pressure sensor.

sensors A, B, C). Pressure transmitter A faces the lower reservoir and measures the water-level height when the system is not running. The pressure transmitter C is always in communication with the upper reservoir measuring its water-level when the valve is closed. The water-level height measure needs to be continuously calibrated to the atmospheric pressure.

Every test begins with recording the water levels of the reservoirs to provide the initial theoretical available head (gap from transmitters C and A in Fig. 10). Once the machine starts the valve is progressively set open at 100%. From then on, until the closing of the valve, sensors A and B define the available head. Water starts flowing in the piping system and, due to friction, energy losses are encountered: the available head is now reduced by a factor dependent on the square of the flow rate. The plot on the total pressure development shows that the available head is really affected by the working conditions up to a shortening of 23%.

For the exploration of the entire operating range in pump and turbine modes, multiple tests are conducted. The efficiency is defined as the power transferred between the available hydraulic power to the shaft

$$\eta_p = \frac{\rho g\, H_p Q_p}{M \omega_p} \qquad \eta_t = \frac{M \omega_t}{\rho g\, H_t Q_t} \tag{10}$$

where ω is the rotational speed in rad/s and M is the torque in Nm. Eq. (9) includes mechanical losses in the shaft seals and bearings, and the volumetric efficiency.

The logic of energy management of the μ-PHES is realised by a PLC connected to a computer. The rationale for the management approach in the smart grid is based on the characterisation of the pump performances (in pump and turbine modes) and the continuous evaluation process of the grid energy fluxes. Table 2 summarised the key points for a correct functioning of the μ-PHES installed.

3. Experimental characterisation

The use of variable speed pumping in PHES integrated into a smart

grid aims to give flexibility to energy storage. Whenever possible the pumping station only uses the intermittent and fluctuating surplus energy from the rest of the system. The manometric head provided by a pump or exploited by a PaT is dependent on the rotation speed of the impeller. For this reason, one method to adapt the characteristic curves of a turbomachine with fixed geometry is to change its peripheral speed. The hill chart in Fig. 11 shows the characteristic curves of a pump installed on the site in Froyennes at different rotational speeds from 800 to 1100 rpm. Peak efficiency is measured as being 72.7%. The mechanical power consumption is thus re-traceable according to Eq. (9) and is shown in Fig. 12. The pump can use a relatively wide range of electrical power moving from 5 kW (low speed) up to almost 17 kW (high speed) for storing energy in the upper reservoir.

As speed changes, efficiency follows a parabolic curve with apexes at the origin. Efficiency is therefore independent of limited changes in rotational speed except for a slight shift dependent on the Reynold number. Minimum operating pump shaft speed is defined as that at which the pumping system is no longer able to deliver a positive flow rate against a static head. The maximum speed is linked to the maximum flow rate on the $H - Q$ curve which limits the operation due to cavitation and mechanical constraints. Hence, it is specific to each working condition. The minimum operating speed of the installed pump is 65% when the lower reservoir is full (minimum geodetic head) and 90% when the lower reservoir is about to be empty (minimum geodetic head).

The primary goal of using PaT with variable speed is to maintain a nearly constant high efficiency regardless of the head availability. In practice the two water levels are always changing, mostly because of the considerable depth of the lower reservoir. In reverse mode, the efficiency is higher than 70% over all the available head range offered by the site. Consequently, the rotational speed must be adapted up to 800 rpm (Fig. 13). Finally, a round-trip hydraulic efficiency of 52% is achieved by the experimental investigation in pump mode and turbine mode.

The PaT characteristic curves are showed in Fig. 14 which compares the efficiency curves obtained by the measurement at fixed speed N_{PaT} with a variable regulation of 500–800 rpm. The black line is the efficiency curve of the PaT as it would run at the pump nominal synchronous speed N_{PUMP} and displays the relevant efficiency improvement of using speed adjustment. The runaway curve, where $M = 0$, limits the area of energy production as already depicted in Fig. 13. The range of flow rate at high efficiency (>70%) in reverse mode is 1.2 times larger than in pump mode regardless of the reduced speed: 65–105 kg/s in pump mode and 80–135 kg/s in turbine mode. At minimum load conditions, the PaT runs with a geodetic head reduction of about −55% from its maximum. Lower rotational speed allows the PaT to adapt to the running water regime at reduced available head and to preserve high efficiency.

The motor generator is a 30 kW WEG type 380/660 V 50 Hz 6P and

Table 1
Instrumentation range and accuracy summary.

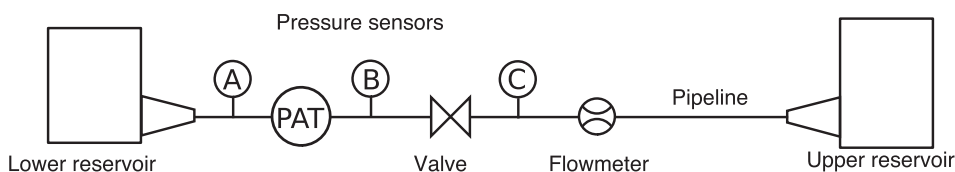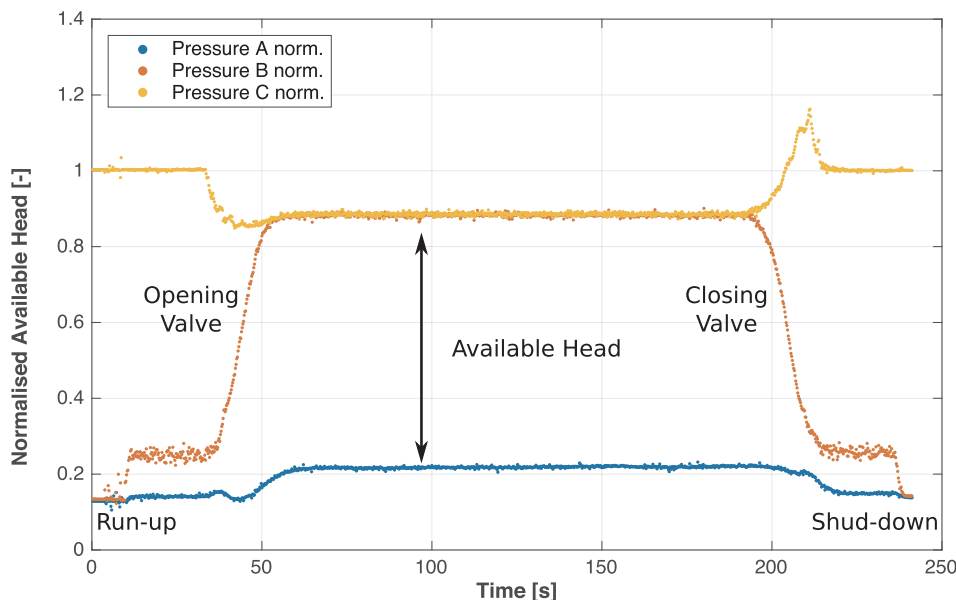| Apparatus	Quantity	Sensor type	Sensor Range	Sensor Accuracy
SPT100	T_{IN}	Static temperature	0–50 °C	± (0.3 + 0.005 $|T|$°C)%
	T_{OUT}	Static temperature	0–50 °C	
DATAFLEX32/300	M	Torque-meter	±300 Nm	±0.2% FS
	N	Rotational speed	0–2000 rpm	
Diris60A	P_{syt}	Wattmeter	Scalable	±0.5%
UNIK 5000	P_A	Pressure sensor	−0.9 to 0.6 bar	±0.2% FS
	P_B	Pressure sensor	0–2.0 bar	
	P_C	Pressure sensor	0–1.5 bar	
AquaTrans T600	$\dot{m}$	Ultrasonic flow-meter	±150 kg/s	±1.5% FS

Fig. 9. Schematic layout of the set-up.

Fig. 10. Pressure measurements for sensor A, B and C facing PaT run-up, opening valve, normal operation, closing valve and shut-down.

it is characterized by an efficiency of 92.1–92.8% in the range of 50–100% of the load. The total effect of the motor/generator and the VFD is presented in Fig. 15. In pump mode, the total efficiency does not differ substantially from the motor manufacturer data-sheet. However, in turbine mode, the driver lowers the total electric efficiency and differently according to the speed. The overall efficiency of the system including charge, discharge and conversion turns out to be 42%. The round-trip efficiency obtained for the installed μ-PHES is not comparable with large scale PHES of near 80% [62] or lithium batteries (65–93%) [63].

Fig. 16 presents the system operation and modelled performance on the 21st of April 2017. This day could be considered as a typical week-day of the month of April. The load diagram shows the intense use of

heating and ventilation system from the early morning, when the first consumption peak occurs. With real-time power measurements, as used in μ-PHES set-up (Section 2.4), the surplus of energy is assigned directly to the pump and used in charging the upper reservoir. The rotational shaft speed is modulated as well as it suits with the actual available water levels. The pump operates in reverse mode (negative rpm) when the PV groups and wind turbines do not cover the electricity demand. The fluctuations of the turbine rotational speed indicate that there are periodically operating changes according to the imposed frequency of PLC command loop (Table 2). The upper reservoir is emptying and the lower reservoir is filling-up: the available head decreases progressively. Interestingly, the hydraulic efficiency is maintained at its maximum until the completed cycle (about 70%).

Table 2
Summary of PHES command actions.

Step	Description
Check instrumentation	Check on alarms, Voltage and consistency of the measurements
Measurements	The acquisition data system is running in continuous for real time control and command
Evaluation of energy surplus	Instant difference of load demand and RES production With positive surplus, pump is ready in pump-mode With negative surplus, pump is ready in turbine-mode Evaluate the requirements[a]
Detection of the water levels	Definition of the stationary head among the two reservoirs
Mapping	Forecast the working conditions based on surplus and water levels (rpm, m^3/s) Estimate losses and compute the available head Re-assess the operating condition and requirements
Run-up	The pump runs (pump-mode or turbine-mode)
Synchronisation	Rotational speed adjustments based on available head fluctuation and instant energy surplus
Shut-down	Operating conditions or requirements are no longer met
Stand-by	Maintain the system ready

[a] Water levels of both reservoirs in the limits agreed under security and safety reasons.
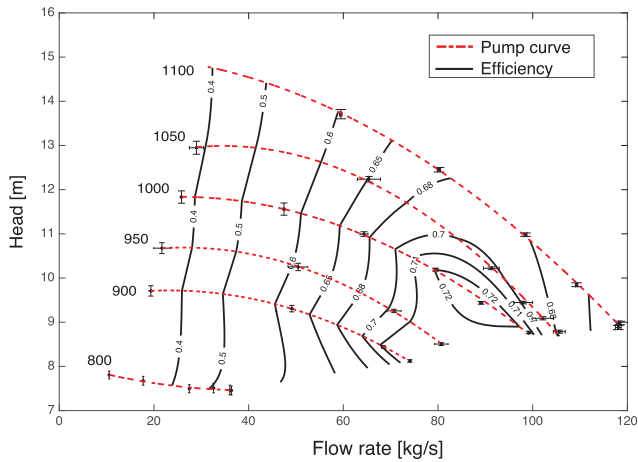
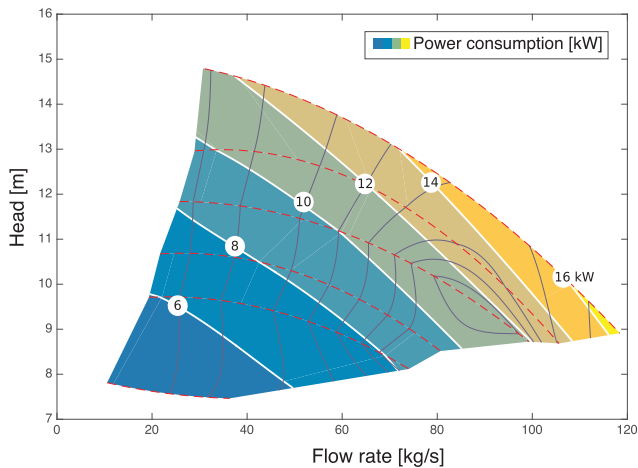**Fig. 11.** Experimental results of the pump characteristics and its hydraulic efficiency.

Fig. 12. Experimental results of the pump and its power consumption.
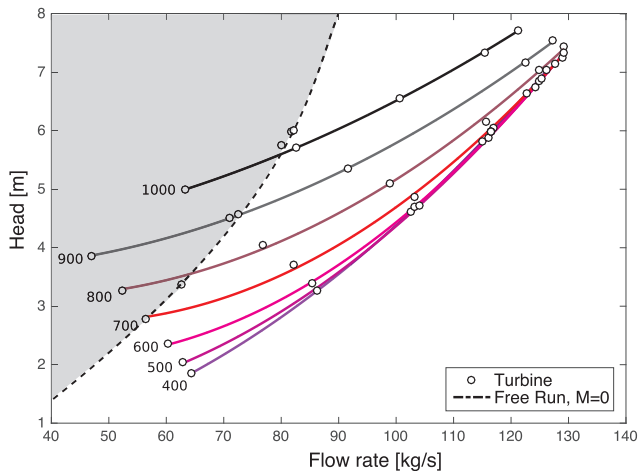

Fig. 13. Experimental results of PaT characteristics in Q-H plot limited by the runaway curve.

4. Cost-benefit analysis

The Levelised Cost of Energy (LCOE) is a method to evaluate the economic value of an energy project. It provides the price per energy unit (€/kWh) that balances out all the costs of the project. All the costs incurred are divided by all the energy provided along the project
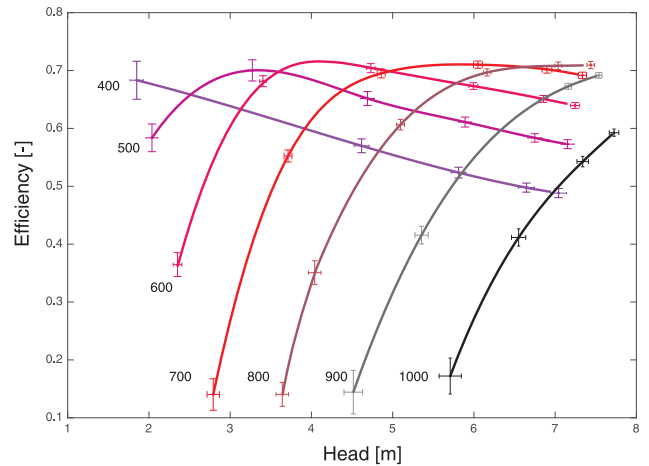

Fig. 14. Experimental results on PaT efficiency over the variable head, *H*.

duration, *K* (years). The values must take into account the time-varying value of money with the real yearly discount rate, *d* (%). The LCOE is obtained by

$$LCOE = \sum_{k=0}^{K} \frac{C_k/(1 + d)^k}{E_{out}/(1 + d)^k} \tag{11}$$

where C_k is the cost in the year k in €, E_{out} is the energy output in year k in kWh. The lifetime span, K, (35 years), the yearly degradation in efficiency of the system (-0.2%/year) and the operation and maintenance (O&M) yearly cost (30 €/kW/year) are sensitive parameters in the LCOE calculation. The electricity required for charging the upper reservoir is fully provided by the surplus of the Renewable Energy Sources (RES) systems installed on site whose costs are already considered amortised. The RES on site are not meant to be connected to the grid and the injection of excess power into the grid is therefore not possible. The PHES operating control is able to match with the instant available head value, *H*, and, if possible, start the pump at the most suitable rotational operating speed with the exact surplus of power generated by RES in Negundo. For the LCOE calculation of the μ-PHES in Negundo, the capital costs of the first year are equal to about 108 k€, with 42% going to pipeline related costs and 26% for the motor-pump group coupled with the electric driver. The collected list of costs includes materials, accessories and manpower. The reservoir costs are not applied in this calculation because one already exists as a storm-water basin and the other one is considered as an extension of the first. The use of a storm-water basin as a reservoir is an important cost-effective solution. According to the type of implemented tank [11], the equivalent cost for a 625 m³ reservoir would have laid between 43–187 k€, translating into an expense reduction of 28–61%.

In order to avoid the necessity to pay for electricity to charge the reservoir in Negundo, the use of RES is crucial to reach a high number of PHES cycles and the targeted LCOE value. The PV panel and wind turbine capacity factor (Table 3), defined as the ratio of the power generated and the rated peak power, drastically affects the annual energy yield and leads to the possibility of an over-dimensioned RES installation.

In Fig. 17 the daily and monthly average of the capacity factor for PV panels in Belgium is shown for the months of April, July, October and December 2017 [64]. More than one daily full cycle is possible as plotted as an example in Fig. 18. The electricity load consumption is mainly due to the heating, ventilation, and air conditioning systems of the adjacent buildings. The load fluctuates at high peak during weekdays with reduced consumption during Saturday and Sunday. Both PV and wind energy production is formulated as a monthly average taking into account the associated capacity factor. During night time the RES power production drops to the wind turbine contribution only, which
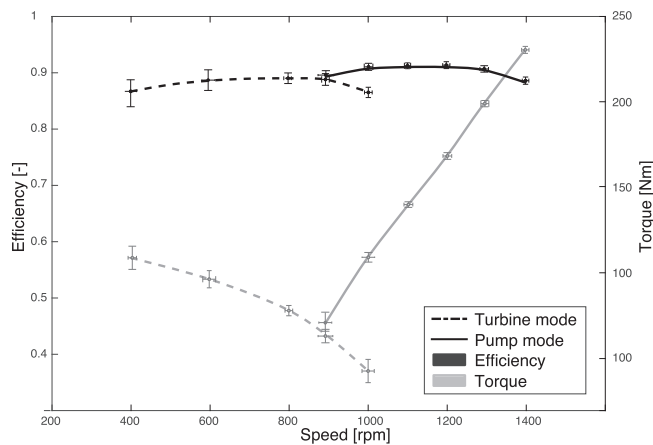
Fig. 15. Electrical efficiency and torque over the variation of the rotational speed for turbine and pump modes.
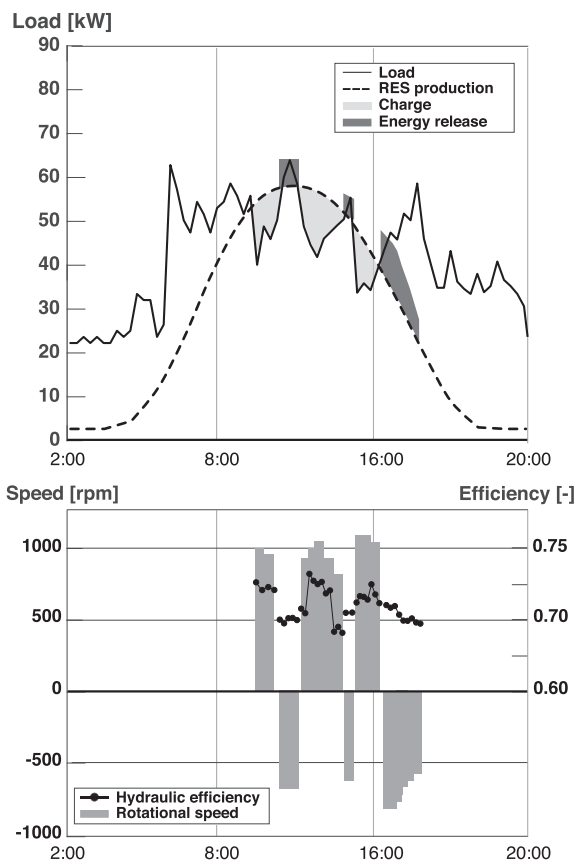

Fig. 16. Absorbed and produced power by the storage system according to the load profile and RES production. Related rotational speed and hydraulic efficiency values between 02:00 and 0:00 (April 2017).

Table 3

Averaged capacity factor for the PV panels and wind turbines in Belgium 2017. Data extracted from [64].

Period	PV capacity Factor	Period	Wind turbine Capacity factor
April	0.74	Spring	0.27
July	0.67	Summer	0.22
October	0.61	Fall	0.26
December	0.43	Winter	0.29

results be very limited. With an averaged regime of 1.5 cycle per day, the LCOE calculated is equal to 1.06 €/kWh.

Fig. 19 shows a specific sensitivity analysis for the variation of certain parameters over a range of ± 20%. As expected, it emerges that LCOE can be reduced significantly by raising the total energy output, improving efficiency and/or exploiting a higher available head. Pumps with a hydraulic efficiency higher than about 70% are available for this power size. Presumably they also have a higher efficiency in reversed mode. A longer lifetime, K, also has a positive effect on the final LCOE. Obviously, the capital cost has a big impact and should be reduced in order to reach grid price parity. Directional drilling cost is an exceptional expense that it was required for these specific cases: 26% of the total capital cost in Negundo. Furthermore, the pipeline cost is relevant here due to the ratio of pipeline length and geodetic head L/H in the Negundo layout which is about 8. In a hydropower system L/H can often be smaller than 3 and thus it underlies the considerable scope for improvement in this subject for other future μ-PHES. O&M costs have quite a limited influence on the total outcomes: the most common practises on site are to routinely inspect and maintain the trash rack cleaning systems so as to keep the aspiration and discharge channels free of any major obstructions. With the methodology developed and the data analysis available, it is possible to propose a second case study.

From Eq. (1), it appears that a larger available head makes the hydropower plant more energy proficient with the same amount of stored water. Assuming that a six-story building is situated at the ground level of the upper reservoir in Froyennes, its rooftop could provide the space for an upper reservoir 20 meters higher than the previous one. The dimensions and structure of the roof would respect the limits defined by the minimum load according to the law (1500 kg/m²) [65]. 800 m² are sufficient for a total water volume of 625 m³. However, the roof surface must be adapted from the standard coating with a reinforcement waterproofing of about 36 €/m² as defined by the contractor. This extra cost could be mitigated by possible synergies in the building's water infrastructure. External open-air tanks are subjected to environmental phenomena and are not always suitable for a potable water network. However, they can find valid applications for rainwater harvesting and fire safety systems. Today, Belgian national legislation requires that all new constructions have a rainwater harvesting system that can be used for toilet flushing and external water uses [66]. This legislation has been devised to help reduce the demand for mains supply water and to collect and use rainwater as part of sustainable drainage systems [66]. In this case study the pipeline needs to be extended a further 20 meters to reach the roof of the building adding some extra costs. The flow rate is considered to remain equal to the μ-PHES in Froyennes but the new available head requires selecting a PaT with lower specific speed (Eq. (3)). As the specific speed decreases, the ratio of impeller diameter to impeller eye diameter increases. As a consequence, a larger radial extension blade is required. However, the water flow rate is the same, and the flanged diameter on the discharge and suction side are thus unchanged. This means that only a different impeller shape of whole pump-block needs to be changed. The pump price is not drastically higher, but the motor and driver must be able to manage a larger electric load. The new costs have been estimated by the constructor and summarized in the Table 4. The PaT and pump hydraulic efficiency in the case study are considered equal to those in the Negundo site.

The results of the LCOE calculations against the number of PHES full cycles is plotted in Fig. 20 and are compared with other storage technologies. In this plot, lead-acid batteries shall be regarded as having an efficiency of 80% [67], a capital cost of 600 €/kWh and the lifespan of 4 years [11]. Besides the higher capital cost of about 1000 €/kWh [11], more competitive LCOE is obtained with lithium-ion batteries due to their durability of about 18 years and an efficiency of 90% [67]. It appears that PHES is the most cost-effective storage technology in long-term and for large scale application [62]. However, micro PHES meets different outcomes. The μ-PHES operative in Froyennes appears to be
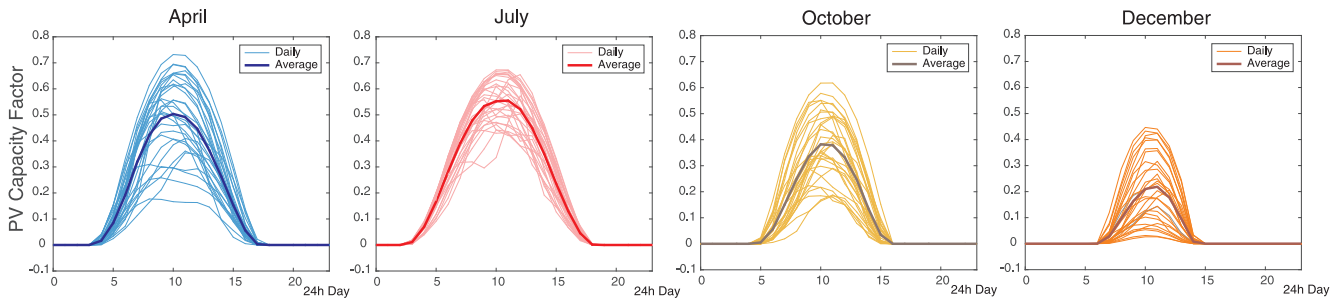
Fig. 17. PV panels capacity factor in Belgium 2017 during the month of April, July, October and December. Data extracted from [64].

competitive with other storage technologies with a high number of charging/discharging cycle per year: 2 cycles and 3 cycles per day is required to obtain an LCOE that is competitive with lead-acid battery storage (0.78 €/kWh) and lithium-ion battery storage (0.45 €/kWh).

5. Conclusions

In Europe and most of the world the main challenge of recent energy policy is to increase the share of RES with the aim of reducing greenhouse gas emissions to 80–95% below 1990 levels by 2050 [69]. In this context, energy storage plays a crucial role. For PV panel systems, capacity factors lead towards over-dimensioning RES plants in order to be able to satisfy energy demand even on cloudy days. To tackle this challenge it appears necessary to develop a large storage capacity and deal with issues caused by the mismatch between energy production and consumption, most often occurring on sunny days. These problems become consistent for grid stability and are particularly acute for hourly or sub-hourly operators in the energy markets.

Regarding PHES, large-scale power plants have made significant efforts towards flexibility in order to provide grid frequency stability supported by a significant share of intermittent RES. In small scales PHES, the target is to improve the energy efficiency of decentralized energy sources which are currently growing rapidly at a residential and industrial level. The major difficulties for the feasibility of μ-PHES are the low energy capacity of the system which is limited by the maximum available height differential of the reservoirs, and the high costs involved. Also, the global efficiency and economic feasibility are importantly affected by the response of pumps and turbines to load variation. To face the frequent constraints linked to the site location and load variation, innovative options must be analysed and tested to better evaluate the potential of PHES at micro scales. The description of the site here presented provides technical insights into micro PHES research and into reversible pump applications. The experimental results and data obtained on site allow for cost improvements and contribute to the awareness of μ-PHES performance and feasibility.

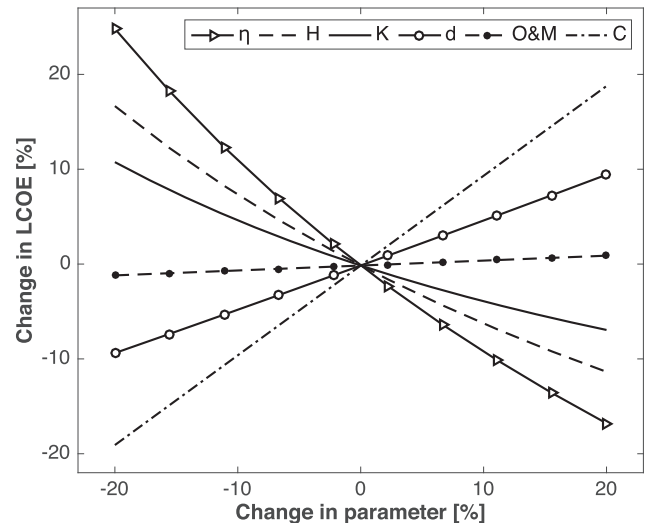The μ-PHES in Negundo described in this paper adopts a single

Fig. 19. LCOE sensitivity analysis of the μ-PHES in *Quartier Negundo*.

centrifugal PaT for both pumping and generating phases. By using VFD the pump can operate in normal and reverse modes to maintain the highest hydraulic efficiency over a range of 40–120% of the nominal load design. At such extreme working conditions, a standard hydraulic turbine at fixed rotational speed is subjected to cavitation and instability both of which reduce the performance. The maximum efficiency measured in reversed mode is approximately 1–2% less than the efficiency of the turbomachine in pump mode. With a peak of 71%, the PaT hydraulic efficiency recorded is smaller than with regular micro turbines [18,21], but still very competitive at this power-size.

The use of the same machine for pumping and generating represents an outstanding solution in savings cost energy, space and maintenance. A cost-benefit analysis proves that the installed μ-PHES have not reached parity to other small scales energy storage, but yet the results are promising. A significant reduction in cost investment is reached by
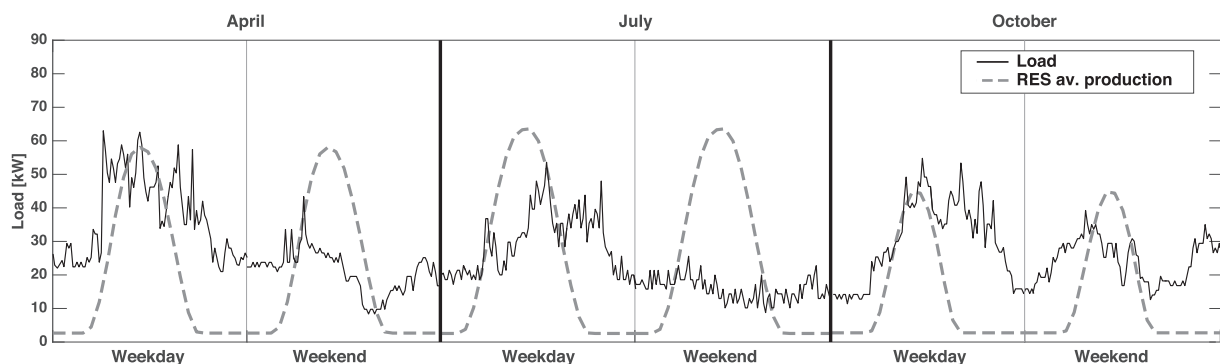

Fig. 18. Load consumption of *quartier Negundo* during weekdays and weekends and averaged empowered RES production on site (PV and wind turbines) in April, July and October 2017, by way of example.

Table 4
Capital costs for μ-PHES in *quartier Negundo* and cost estimation for the second case study.

|	Quartier Negundo [€]		Case study [€]	
Motor-pump group	12,900		18,000	
Frequency drive	15,600	26%	40,000	33%
Electric panel and control	19,700		19,700	
Electro mechanic valve	1700		1700	
Acquisition data system	2300		2300	
Connections and cables	2100	24%	2100	15%
Directional Drilling	28,400		28,400	
Pipeline	17,300	42%	24,400	30%
Upper reservoir	–		28,800	17%
Others	8300	8%	8300	5%
Total	108,300	100%	173,700	100%
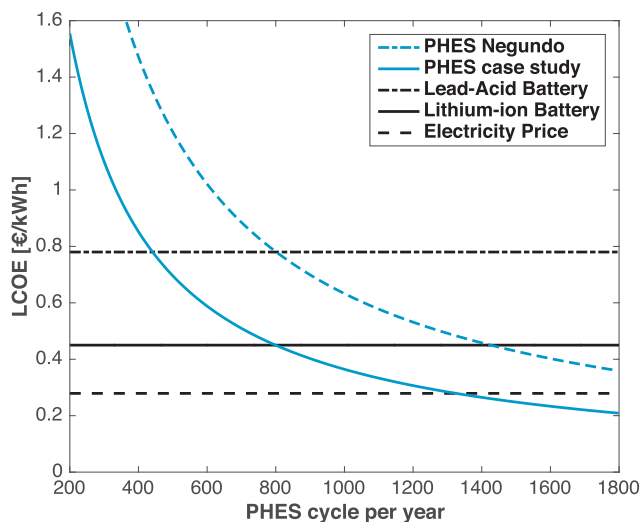
Fig. 20. LCOE comparison of the PHES in Negundo with other technologies and the electricity price in Belgium for household consumers in 2017 (0.2877 EUR per kWh) [68].

using an already existing storm-water basin on site, by reducing the construction costs of at least 28%. A LCOE of 1.06 €/kWh is obtained for the micro PHES realised in Negundo, but for the same amount of cycles per year it could reach 0.58 €/kWh, as showed in the further case study. The latter shows possible additional improvements linked to the specificity of the site: cutting costs and increasing the total energy output, E_{out}, by increasing the exploitable available head. Moreover, the LCOE sensitivity analysis here discussed provides a rational basis for making the most economically informed decision, possibly leading to more future inspirations within the academic and professional communities.

Acknowledgements

References

[1] IRENA. International Renewable Energy Agency, 2018.
[2] Höglund-Isaksson L, Winiwarter W, Purohit P, Rafaj P, Schöpp W, Klimont Z. EU low carbon roadmap 2050: Potentials and costs for mitigation of non-CO2greenhouse gas emissions. Energy Strategy Rev 2012;1(2):97–108. https://doi.org/10.1016/j.esr.2012.05.004.
[3] Rehman S, Al-Hadhrami LM, Alam MM. Pumped hydro energy storage system: A technological review. Renew Sustain Energy Rev 2015;44:586–98. https://doi.org/10.1016/j.rser.2014.12.040.
[4] Dostál Z, Ladányi L. Demands on energy storage for renewable power sources. J Energy Storage 2018;18:250–5. https://doi.org/10.1016/j.est.2018.05.003.
[5] Sandia National Laboratories. DOE global energy storage database, http://www.energystorageexchange.org, 2018 [Accessed 03 July 2018].
[6] Gimeno-Gutiérrez M, Lacal-Arántegui R. Assessment of the European potential for pumped hydropower energy storage based on two existing reservoirs. Renew Energy 2015;75:856–68. https://doi.org/10.1016/j.renene.2014.10.068.
[7] Yang CJ, Jackson RB. Opportunities and barriers to pumped-hydro energy storage in the United States. Renew Sustain Energy Rev 2011;15(1):839–44. https://doi.org/10.1016/j.rser.2010.09.020.
[8] Spänhoff B. Current status and future prospects of hydropower in Saxony (Germany) compared to trends in Germany, the European Union and the World. Renew Sustain Energy Rev 2014. https://doi.org/10.1016/j.rser.2013.10.035.
[9] Manolakos D, Papadakis G, Papantonis D, Kyritsis S. A stand-alone photovoltaic power system for remote villages using pumped water energy storage. Energy 2004;29(1):57–69. https://doi.org/10.1016/j.energy.2003.08.008.
[10] Stoppato A, Benato A, Destro N, Mirandola A. A model for the optimal design and management of a cogeneration system with energy storage. Energy Build 2016;124:241–7. https://doi.org/10.1016/j.enbuild.2015.09.036.
[11] de Oliveira e Silva G, Hendrick P. Pumped hydro energy storage in buildings. Appl Energy 2016;179:1242–50. https://doi.org/10.1016/j.apenergy.2016.07.046.
[12] IEA IEA. Global EV Outlook 2017: Towards cross-modal electrification. IEA Publications; 2017. https://doi.org/10.1787/9789264277882-en. p. 1–71.
[13] Nourbakhsh A, Derakhshan S, Javidpour E, Riasi A. Centrifugal & axial pumps used as turbines in small hydropower stations. Hidroenergia 2010: International congress on small hydropower international conference and exhibition on small hydropower. 2010. p. 16–9.
[14] Carravetta A, Del Giudice G, Fecarotta O, Ramos HM. Energy production in water distribution networks: A PAT design strategy. Water Resour Manage 2012;26(13):3947–59. https://doi.org/10.1007/s11269-012-0114-1.
[15] Carravetta A, Del Giudice G, Fecarotta O, Ramos HM. Pump as turbine (PAT) design in water distribution network by system effectiveness. Water (Switzerland) 2013;5(3):1211–25. https://doi.org/10.3390/w5031211.
[16] Capelo B, Pérez-Sánchez M, Fernandes JF, Ramos HM, López-Jiménez PA, Branco PJ. Electrical behaviour of the pump working as turbine in off grid operation. Appl Energy 2017. https://doi.org/10.1016/j.apenergy.2017.10.039.
[17] Orchard B, Klos S. Pumps as turbines for water industry. World Pumps 2009;2009(8):22–3. https://doi.org/10.1016/S0262-1762(09)70283-4.
[18] Paish O. Micro-hydropower: Status and prospects. Proc Inst Mech Eng, Part A: J Power Energy 2002;216(1):1–40. https://doi.org/10.1243/095765002760024827.
[19] Motwani KH, Jain SV, Patel RN. Cost analysis of pump as turbine for pico hydropower plants - A case Study. Procedia engineering, vol. 51. 2013. p. 721–6. https://doi.org/10.1016/j.proeng.2013.01.103.
[20] Binama M, Su WT, Li XB, Li FC, Wei XZ, An S. Investigation on pump as turbine (PAT) technical aspects for micro hydropower schemes: A state-of-the-art review. Renew Sustain Energy Rev 2017;79:148–79. https://doi.org/10.1016/j.rser.2017.04.071.
[21] Jain SV, Patel RN. Investigations on pump running in turbine mode: A review of the state-of-the-art. Renew Sustain Energy Rev 2014;30:841–68. https://doi.org/10.1016/j.rser.2013.11.030.
[22] Williams A. The turbine performance of centrifugal pumps: a comparison of prediction methods. Proc Inst Mech Eng, Part A: J Power Energy 1994;208(1):59–66.
[23] Pugliese F, De Paola F, Fontana N, Giugni M, Marini G. Experimental characterization of two Pumps As Turbines for hydropower generation. Renew Energy 2016;99:180–7. https://doi.org/10.1016/j.renene.2016.06.051.
[24] Nautiyal H, Kumar A, Yadav S. Experimental investigation of centrifugal pump working as turbine for small hydropower systems. Energy Sci Technol 2011;1(1):79–86. https://doi.org/10.3968/j.est.1923847920110101.006.
[25] Ciocan GD, Teller O, Czerwinski F. Variable speed pump-turbines technology. UPB Scientific Bul, Series D: Mech Eng 2012. https://doi.org/10.1111/j.2042-3306.1984.tb01832.x.
[26] Chazarra M, Pérez-Díaz JI, García-González J, Praus R. Economic viability of pumped-storage power plants participating in the secondary regulation service. Appl Energy 2018. https://doi.org/10.1016/j.apenergy.2018.02.025.
[27] Pérez-Díaz JI, Chazarra M, García-González J, Cavazzini G, Stoppato A. Trends and challenges in the operation of pumped-storage hydropower plants. Renew Sustain Energy Rev 2015. https://doi.org/10.1016/j.rser.2015.01.029.
[28] Yang W, Yang J. Advantage of variable-speed pumped storage plants for mitigating wind power variations: Integrated modelling and performance assessment. Appl Energy 2019;237:720–32. https://doi.org/10.1016/j.apenergy.2016.06.097.
[29] Steimes J, Hendrick P, Haut B, Doucement S. Cost and revenue breakdown for a pumped hydroelectric energy storage installation in Belgium. Sustainable hydraulics in the era of global change – proceedings of the 4th european congress of the international association of hydroenvironment engineering and research, IAHR 2016 2016. https://doi.org/10.1201/b21902-49.
[30] Witt A, Chalise DR, Hadjerioua B, Manwaring M, Bishop N. Development and implications of a predictive cost methodology for modular pumped storage hydropower (m-psh) projects in the united states, 2016.
[31] Pujades E, Orban P, Bodeux S, Archambeau P, Erpicum S, Dassargues A. Underground pumped storage hydropower plants using open pit mines: How do groundwater exchanges influence the efficiency? Appl Energy 2017;190:135–46.

https://doi.org/10.1016/j.apenergy.2016.12.093.

[32] Poulain A, de Dreuzy JR, Goderniaux P. Pump Hydro Energy Storage systems (PHES) in groundwater flooded quarries. J Hydrol 2018. https://doi.org/10.1016/j.jhydrol.2018.02.025.

[33] Anilkumar TT, Simon SP, Padhy NP. Residential electricity cost minimization model through open well-pico turbine pumped storage system. Appl Energy 2017. https://doi.org/10.1016/j.apenergy.2017.03.020.

[34] Carravetta A, Fecarotta O, Ramos HM. A new low-cost installation scheme of PATs for pico-hydropower to recover energy in residential areas. Renew Energy 2018. https://doi.org/10.1016/j.renene.2018.02.132.

[35] Barbour E, Wilson IA, Radcliffe J, Ding Y, Li Y. A review of pumped hydro energy storage development in significant international electricity markets. Renew Sustain Energy Rev 2016. https://doi.org/10.1016/j.rser.2016.04.019.

[36] Aneke M, Wang M. Energy storage technologies and real life applications? A state of the art review. Appl Energy 2016. https://doi.org/10.1016/j.apenergy.2016.06.097.

[37] Deane JP, Ó Gallachóir BP, McKeogh EJ. Techno-economic review of existing and new pumped hydro energy storage plant. Renew Sustain Energy Rev 2010. https://doi.org/10.1016/j.rser.2009.11.015.

[38] Nourbakhsh A, Jaumotte A, Hirsch C, Parizi HB. Turbopumps and pumping systems. Springer Science & Business Media; 2007.

[39] ANDRITZ, https://www.andritz.com/resource/blob/34004/fd9cdefb249b7fa645228add62d9aa26/hy-andritz-pumps-as-turbines-en-data.pdf, 2019.

[40] SULZER, https://www.sulzer.com/en/shared/applications/2017/05/29/09/07/hydraulic-power-recovery-turbine, 2019.

[41] Pérez-Sánchez M, Sánchez-Romero FJ, Ramos HM, López-Jiménez PA. Energy recovery in existing water networks: Towards greater sustainability. Water (Switzerland) 2017. https://doi.org/10.3390/w9020097.

[42] Morabito A, Steimes J, Hendrick P. Pumped hydroelectric energy storage: A comparison of turbomachinery configurations. Sustain Hydraul Era Global Change 2016:261–8. https://doi.org/10.1201/b21902-48.

[43] Singh P, Nestmann F. An optimization routine on a prediction and selection model for the turbine operation of centrifugal pumps. Exp Thermal Fluid Sci 2010;34(2):152–64. https://doi.org/10.1016/j.expthermflusci.2009.10.004.

[44] Alatorre-Frenk C, Thomas T. The pumps as turbines approach to small hydropower. World congress on renewable energy, Reading. 1990.

[45] Childs S. "Convert pumps to turbines and recover hp. Hydrocarbon Process Petrol Refiner 1962;41(10):173–4.

[46] Schmiedl E. Serien-kreiselpumpen im turbinenbetrieb. Karlsruhe, Germany: Pumpentagung; 1988.

[47] Sharma K. Small hydroelectric projects – use of centrifugal pumps as turbines. Bangalore, India: Kirloskar Electric Co.; 1985.

[48] Stepanoff AJ. Centrifugal and axial flow pumps: theory, design, and application. New York: Wiley; 1957.

[49] Lewinsky-Kesslitz H. Pumps as turbines for small-scale hydropower plants. WASSERWIRTSCHAFT 1987;77(10):531–7.

[50] Derakhshan S, Nourbakhsh A. Experimental study of characteristic curves of centrifugal pumps working as turbines in different specific speeds. Exp Thermal Fluid Sci 2008;32(3):800–7. https://doi.org/10.1016/j.expthermflusci.2007.10.004.

[51] Derakhshan S, Nourbakhsh A. Theoretical, numerical and experimental investigation of centrifugal pumps in reverse operation. Exp Thermal Fluid Sci 2008;32(8):1620–7. https://doi.org/10.1016/j.expthermflusci.2008.05.004.

[52] Barbarelli S, Amelio M, Florio G. Predictive model estimating the performances of centrifugal pumps used as turbines. Energy 2016;107:103–21. https://doi.org/10.1016/j.energy.2016.03.122.

[53] Morabito A, Steimes J, Bontems O, Al Zohbi G, Hendrick P. Set-up of a pump as turbine use in micro-pumped hydro energy storage: A case of study in Froyennes Belgium. J. Phys.: Conf. Ser. vol. 813. 2017. https://doi.org/10.1088/1742-6596/813/1/012033.

[54] Buckingham E. On physically similar systems; Illustrations of the use of dimensional equations. Phys Rev 1914;4(4):345–76. https://doi.org/10.1103/PhysRev.4.345.

[55] IEC. Hydraulic turbines, storage pumps and pump- turbines-model acceptance tests. IEC 60193 Standard - International Electrotechnical Commission Geneva; Nov. 1999. p. 578.

[56] Gulich JF. Centrifugal pumps. 2nd ed. Springer; 2010.

[57] Engeda A. Auswahl von Kreiselpumpen als Turbinen. Pumpentagung Karlsruhe 1988;A6.

[58] Schmiedl E. Pumpen als turbinen. Pumpentagung, Karlsruhe (A6) 1988.

[59] Yang C. Performance of the vertical turbine pumps as hydraulic turbines. Proc Performance Charact Hydraulic Turb Pumps 1983.

[60] IEC. Technical report: Hydraulic turbines, storage pumps and pump-turbines – Tendering Documents - Part 2: Guidelines for technical specifications for Francis turbines (IEC TR 61366-2:1998); 1998.

[61] Otero L, Sanz PD. High-pressure shift freezing. Part 1. Amount of ice instantaneously formed in the process. Biotechnol Prog 2000;16(6):1030–6. https://doi.org/10.1021/bp000122v.

[62] Jülch V. Comparison of electricity storage options using levelized cost of storage (LCOS) method. Appl Energy 2016. https://doi.org/10.1016/j.apenergy.2016.08.165.

[63] Tan P, Jiang HR, Zhu XB, An L, Jung CY, Wu MC, et al. Advances and challenges in lithium-air batteries. Appl Energy 2017. https://doi.org/10.1016/j.apenergy.2017.07.054.

[64] Elia.be. "Solar-pv power generation data," http://www.elia.be/en/grid-data/power-generation/solar-power-generation-data/graph, 2018 [Accessed 28 Feb. 2018].

[65] European Committee for Standardization. Eurocode 1: Actions on structures - Part 1-1: General actions - Densities, self-weight, imposed loads for buildings. 2002;2:1–5.

[66] Cornut P, Aubin D, Van Criekingen M, Dubois O, Dessouroux C, Decroly JM. Public, club and individual management of natural resources: The case of domestic rainwater tanks in Belgium. Erde 2006;137(4):273–92.

[67] Ferreira HL, Garde R, Fulli G, Kling W, Lopes JP. Characterisation of electrical energy storage technologies. Energy 2013;53:288–98. https://doi.org/10.1016/j.energy.2013.02.037.

[68] Statistical Office of the European Communities. EUROSTAT: Electricity prices for household consumers - bi-annual data," http://appsso.eurostat.ec.europa.eu/nui/show.do?dataset=nrg_pc_204&lang=en, 2018 [Accessed 03 July 2018].

[69] European Commission. Energy roadmap 2050, 2012. https://doi.org/10.2833/10759.